On the Uncertainty Sources of Drone-Based Outdoor Far-Field Antenna Measurements

Cosme Culotta-López[1], Stuart Gregson[2], Andrian Buchi[1], Carlo Rizzo[1], Diana Trifon[1], Snorre Skeidsvoll[1], Inès Barbary[3], Joakim Espeland[1]

[1]QuadSAT, {ccl, ab, cr, dt, ss, je}@quadsat.com
[2]Next Phase Measurements, stuart.gregson@npmeas.com
[3]European Space Agency (ESA-ESTEC), ines.barbary@esa.int

***Abstract*—Unmanned Aerial Systems (UAS), colloquially known as drones, offer unparalleled flexibility and portability for outdoor and in situ antenna measurements, which is especially convenient to assess the performance of systems in their real-world conditions of application. As with any new or emerging measurement technology, it is crucial that the various sources of error must be identified and then estimated. This is especially true here where the sources of error differ from those that are generally encountered with classical antenna measurement systems. This is due to the larger number of mechanical degrees of freedom, and to the potentially less repeatable and controllable environmental conditions. In this paper, the impact of some of these various error terms is estimated as part of an ongoing measurement validation campaign. A mechanically and electrically time invariant reference antenna was characterized at ESA-ESTEC's measurement facilities which served here as an independent reference laboratory. The reference results were compared and contrasted with measurements performed outdoors at QuadSAT's premises using QuadSAT's UAS for Antenna Performance Evaluation (UAS-APE). While a direct comparison between the measurement results from ESA-ESTEC and QuadSAT delivers information about the various uncertainties within a UAS-APE system in comparison to classical measurement facilities' and the validity of such a system for antenna testing, other tests aim at providing an estimation of the impact of each error source on the overall uncertainty budget, thus paving the way towards a standardized uncertainty budget for outdoor UAS-based sites.**

I. Introduction

The recent explosion in the use of the electromagnetic (EM) spectrum is resulting in a widespread need for the characterization, verification, and quantification of real-world, installed, system performance [1], [2]. Nowhere is this more acute than in the field of communications and radar [3], [4]. Since the late 1930s, huge advances have been made in the characterization, interpretation, and verification of a range of properties associated with the emission, reception and scattering of EM fields. Many practitioners have devoted a great deal of time, effort, and ingenuity to the development of a host of measurement techniques that enable all manner of properties to be determined with a great deal of accuracy and precision [5]–[7].

However almost universally, and perhaps understandably, these have required the use of contrived, very controlled, abstracted environments that exhibit certain specific attributes such as being anechoic, echoic, or some predetermined combination thereof [8]. Unfortunately, this proliferation of competing and coexisting EM-based technologies has resulted in the widely acknowledged need to measure electromagnetically large devices in situ. These devices may either be physically large themselves; or become large and/or are immovable when placed in situ and are taken together with their accompanying supporting structures. These structures may include objects as varied and complex in form as buildings, towers, trains, ships, aircraft, etc. Harnessing existing, conventional, measurement technologies generally require the use of excessively large, uneconomical, or impractical test systems and can often result in measurements that are either inaccurate, incomplete, or in some cases impossible to perform. Such considerations have paved the way for the adoption of alternative, novel approaches that exhibit greater agility, convenience, and cost effectiveness. Thus, the use of drone-based measurement systems has gained increasing attention in recent years in both academia and industry [9]–[11]. One of the principal advantages of employing Unmanned Aerial Systems (UAS), i.e. drones, for antenna measurements is their great flexibility and portability, which renders them ideally suited to in situ measurements. However, the larger number of degrees of freedom such systems provide increases concerns about the positioning and pointing uncertainty mid-flight. Thus, when combined with the need to build confidence in any new technology, this paper will present the results of a recent validation measurement campaign where a mechanically and electrically time invariant reference antenna was characterized at an existing reference

Fig. 1: QuadSAT's compact UAS-APE. The compact gimbaled remote source antenna can be seen situated under the drone.

laboratory, which in this case was ESA-ESTEC's indoor spherical near-field measurement facility [12], and separately using QuadSAT's open-air Unmanned Aerial System for Antenna Performance Evaluation (UAS-APE) test site [13], developed within the framework of a project between QuadSAT and ESA. In this paper, the respective measurement systems will be described before initial results are presented that illustrate the degree of agreement attained between the respective, very different, measurement systems together with an overview of a preliminary uncertainty budget.

II. Unmanned Aerial System for Antenna Performance Evaluation (UAS-APE)

Compared to a conventional far-field test range, the UAS-APE, developed within a research project between QuadSAT and ESA and shown in Fig. 1, with the drone platform, replaces the positioner of traditional ranges for performing antenna measurements. The drone platform has on board an advanced flight controller that, together with the company's proprietary software, enables the user to generate a pre-flight path plan. The path plan is then robustly followed by the controller, rejecting environment disturbances such as wind and gusts, and adjusting drone and propellers velocity in order to guarantee precise path following. At the same time, the RF payload receives navigation data from the drone platform during the flight, and adjusts the three-dimensional pose of the signal source to guarantee correct orientation of the illuminating wave.

A. RF Payload

The RF payload comprises a dual-channel signal source, a probe, a $10\,\mathrm{MHz}$ GPSDO frequency reference, a 3-axis stabilization system, and a microcomputer. The used probe is a dual-polarized quad-ridged horn operating from $6\,\mathrm{GHz}$ to $24\,\mathrm{GHz}$. The purpose of the RF payload is to illuminate the Antenna Under Test (AUT) with a locally quasi-plane wave that maintains precise orientation throughout flight and preserves polarization alignment with the AUT. To achieve this, the signal source is mounted on a 3 axis (yaw-pitch-roll) stabilised gimbal. The orientation estimation in the gimbal is based on sensor fusion and filtering of three different Inertial Measurement Units (IMUs), encoders mounted on the joints of the payload and drone position data. The stabilization and orientation of the signal source is the result of two closely intertwined control loops: an outer control loop receives real-time navigation data from the drone platform, and mathematically computes angles for the motors on the gimbal axes, in order to precisely align the signal source with the AUT; an inner control loop uses on board sensors, such as gyroscopes and accelerometers, to reject external disturbances and dynamic effects of flight, and corrects the orientation angles incoming from the outer loop. The outer loop is executed on the embedded computer on board of the payload, whereas the inner loop is performed at micro-controller level. The embedded computer is also responsible for data collection during the flight, and integration of subcomponent communication protocols.

B. Ground Control Station

The ground control station (GCS) consists of a receiver system, a main computer, and a Real Time Kinematics (RTK) station. The RTK provides positioning error corrections to the UAS-APE through the main computer and a communication module. The GPS receiver on the drone together with the main computer and the RTK corrections, constitutes a Differential Global Positioning System (DGPS) solution, an enhancement with respect to traditional GNSS systems. The DGPS system guarantees UAS position accuracy in the order of a few centimeters with respect to the local reference system of the AUT. In particular, the current RTK system ensures a UAS position accuracy of $2\,\mathrm{cm}$ horizontally and $5\,\mathrm{cm}$ vertically. In other words, the UAS-APE and DGPS system ensures that the stability of the drone platform in a single point is limited to a cube of $30\,\mathrm{cm}$ edge, in conditions of wind of up to 15 m/s ($33\,\mathrm{mph}$ or $54\,\mathrm{km/h}$). The main computer in the GCS interfaces directly with the receiving AUT and performs data collection. This input is combined with drone navigation data, referenced to GNSS time, during the post-flight processing stage, at the end of which the mission dataset is obtained. A mission dataset is an aggregated array where signal levels received by the AUT are expressed with respect to the local AUT reference system, in terms of an azimuth over elevation coordinate system plane. The GCS main computer carries the company proprietary software for automatically performing the post-flight processing stage. The output can then either be directly plotted with the same software, or it can be exported to be used in other applications.

III. Comparison Campaign

A comparison campaign was undertaken in order to assess the accuracy of outdoor measurements using a UAS-APE system and to support the construction of a system uncertainty budget. A lite, compact, offset reflector antenna, MVG SR-40, was chosen as a mechanically and electrically time-invariant test antenna, or AUT, and can be seen in Fig. 2. A reference measurement of the AUT was performed at ESA-ESTEC's facilities, which is then compared to outdoor measurements performed at QuadSAT's using a UAS-APE system. The measurements were performed at a frequency $f = 14.5\,\mathrm{GHz}$.

A. Outdoor range at QuadSAT's facilities

Outdoor measurements were performed in front of QuadSAT's hangar at Hans Christian Andersen airport in Odense, Denmark. The AUT is placed on a 3-axis manual tripod, placed on the ground with a given elevation pointing angle, and a receiver is connected to it, while the UAS-APE works in transmit mode. For this campaign, the UAS-APE system is configured to scan at distances of $r = 350\,\mathrm{m}$ and $r = 700\,\mathrm{m}$. The AUT in the measurement environment is shown in Fig. 2, with the UAS-APE approaching it. Additionally, in Fig. 3, a satellite photo of the measurement site is shown, together

Fig. 2: AUT in the measurement environment, with the UAS-APE approaching it.

Fig. 3: QuadSAT's outdoor range and waypoints of the scanned positions. (Credits: Google Maps)

with the ground-projected waypoints that mark the scanned positions. Although the measurements presented in this work are performed in the range shown, the advantage of this technique is that measurements can be performed virtually anywhere. There is no fixed geometrical reference in the used range: the alignment is performed electrically, which allows the system to be flexible.

B. ESA-ESTEC's CATR

The ESA-ESTEC's CATR (Compact Antenna Test Range) facility [12] is a dual parabolic-cylindrical compact range, which can be used for direct far-field or spherical near-field measurements after moving the position of the transmitting tower inside the test chamber. This allows the accurate measurement of full-sphere antenna patterns and gain. The measurement of the AUT was carried out in this configuration at a frequency of 14.5 GHz. After aligning the positioner of the AUT and the dual-polarized probe, the AUT is aligned mechanically. With the AUT placed in the centre of rotation of the spherical positioner's, the radius of the minimal sphere was measured and used to determine the near-field sample spacing. A polar spherical near-field measurement was taken so that the spherical near-field-to-far-field transformation could be used to calculate the directivity of the antenna, as well as its copolar and cross-polar radiation patterns. A measurement uncertainty budget was also estimated according to the U.S. National Institute of Standards and Technology (NIST) 18-term uncertainty analysis [14], which has become an industry standard for evaluating near-field antenna measurement facilities and their relevant measurement uncertainties.

C. Uncertainty Budget Terms with UAS-APE

Outdoor measurements and, in particular, measurements using UAS suffer from different uncertainty sources than the ones that are typically analyzed for more conventional measurement systems. While some uncertainty sources disappear, others, such as the effect of reflections, are generally more significant and others, such as the alignment and position uncertainty, require different approaches for calculation. The appearance of random errors, such as the ones introduced by random vibrations by the UAS or the effect of wind, also distort the acquired measurement data.
In an effort to pave the way for an uncertainty budget specifically designed for outdoor UAS-based sites, measurements to compensate the effect or derive the impact of several uncertainty sources are performed. To compensate for vibrations and random environmental errors, the same cuts are acquired several times and averaged. To compensate for reflections coming from the environment, the measured cuts are acquired after rotating the AUT by 180 °, for two different distances, and for two different elevation angles of the AUT with respect to the ground. To assess the impact of ground and multiple reflections depending on the distance, radius flights are performed for different scanning angles, whereby the UAS-APE, while pointing towards the AUT, flies away from it or towards it. Using these measurements, the errors presented in the following section are calculated, as well as the impact of the uncertainty terms analyzed in Subsection IV-C. The presented uncertainty budget, however, is only preliminary and consists of a limited number of error sources, laying the ground for future research developments.

IV. Measurement Results

In this section, the results of the measurements acquired as introduced previously are compared and analyzed.

A. Alignment: Raster Scan

As mentioned in Subsection III-A, the measurement alignment is performed electrically, aligning the coordinate system with the boresight of the AUT. To find the maximum of the AUT's main beam and reference the rest of the measurements to it, a raster scan is first performed. The raster scan consists of a series of azimuth cuts acquired over a range of elevation angles in an azimuth-over-elevation coordinate system. During the flight, the trigger is continuously activated, so that the resulting data does not conform to a regular grid. After interpolation of the data to an equispaced grid, the maximum of the main beam is found and used as reference. In Fig. 4, the acquired raster scan is shown, together with the reference data measured at ESA-ESTEC's facilities. Here, the amplitude is presented in the form of a false-colour checkerboard plot. The patterns are tabulated on a regular azimuth over elevation

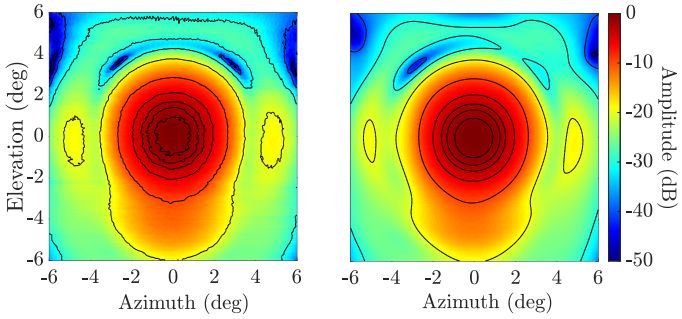

(a) QuadSAT's UAS-APE (b) ESA-ESTEC's facilities

Fig. 4: Measured raster scans.

grid in a relatively narrow angular range about the boresight direction. The plots are generally in good agreement. Differences are expected as a consequence of the outdoor nature of the UAV measurements.

For diagnostic purposes, cuts can be interpolated out of the raster scan performed for alignment. Thereafter, the cuts of interest can be measured again for improved accuracy.

B. Main Cuts

After aligning with the electrical boresight of the AUT, the cardinal cuts, i.e., the AUT's E- and H-plane are acquired. This is repeated on different days, at distances of $r = 350\,\mathrm{m}$ and $r = 700\,\mathrm{m}$, for an elevation angle of the AUT with the ground of $\mathrm{El} = 35°$ and $\mathrm{El} = 45°$, and for the AUT rotated by $180°$ in roll. The data acquired this way is first regularised before the mean is computed. In Fig. 5, the resulting cuts are shown. For the computation of each cut, more than 25 measurements have been used. The Equivalent Error Signal (EES), also shown in Fig. 5, is calculated as

$$\mathrm{EES} = 20\log_{10}\big||E_{\mathrm{Ref.,\,norm}}| - |E_{\mathrm{UAS,\,norm}}|\big|, \qquad (1)$$

where $E_{\mathrm{Ref.,\,norm}}$ and $E_{\mathrm{UAS,\,norm}}$ are the reference pattern measured at ESA-ESTEC and the pattern measured with the UAS-APE system normalized to their maximum, respectively. The mean of the EES for each case is calculated and shown in Table I. Fig. 6 is shown for a better understanding of the impact of a certain EES on a measurement for a defined signal amplitude in dB. The false colour plot illustrates shows the impact of a determined EES, on the horizontal axis, when present for a signal amplitude in dB, given on the vertical axis, in terms of absolute variation in dB form. The contour lines show determined variation values for ease of interpretation.

C. Reduced Uncertainty Budget

Four error sources are considered especially critical for UAS pattern measurements in this work. To calculate the Standard (Std.) uncertainty derived thereof, the following approaches are considered:

1) Environmental Reflections: Radius flights are performed to assess the effect of environmental reflections. The UAS-APE is located at 6 points on the azimuth cut and on 4 points on the elevation cut, as well as at the AUT's boresight, pointing towards the AUT. The measurements are performed

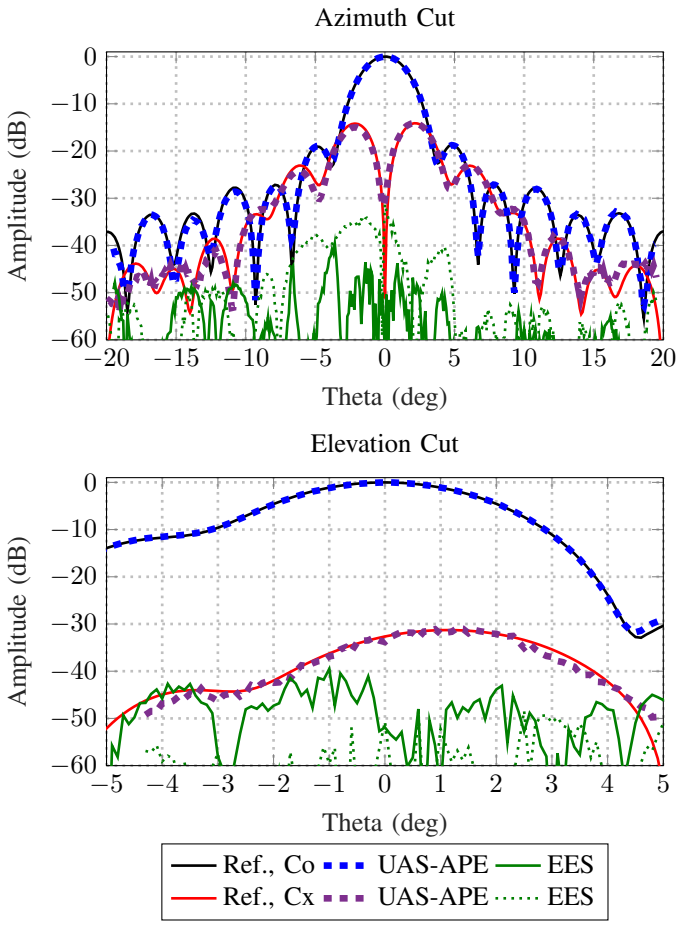

Fig. 5: Measurements of the main cuts, copolar and crosspolar components, together with the EES calculated using the ESA-ESTEC measurements as reference.

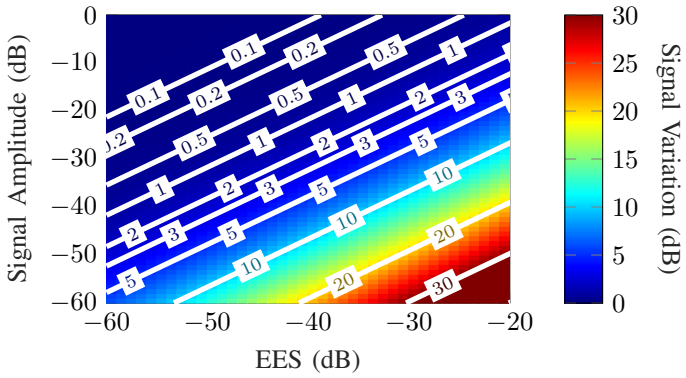

Fig. 6: Impact of a certain EES in terms of variation of a signal of a certain amplitude in dB.

Cut	Co	Cx
Azimuth	−56 dB	−47.5 dB
Elevation	−48 dB	−58 dB

TABLE I: Mean of the EES curves of the main cuts for both polarizations.

Error Source	Dist.	Std. Unc.
Environmental Reflections	V-Shaped	$0.36\,\mathrm{dB}$
Finite Range Length	Uniform	negligible
UAS Positioning	Normal	negligible
Drift	Normal	$0.02\,\mathrm{dB}$
Combined (1σ)		$0.38\,\mathrm{dB}$
Expanded (3σ)		$1.14\,\mathrm{dB}$

TABLE II: Impact of error sources for $14.5\,\mathrm{GHz}$

while changing the distance to the AUT from $r = 50\,\mathrm{m}$ to $r = 700\,\mathrm{m}$, and again reversing the direction of the flight. Each measurement is performed twice per direction. To process the data, the variation in free-space loss is compensated for, and the high-frequency components due to flight vibrations and wind are filtered out in frequency domain, which is computed using a fast Fourier transform. This way, only the ripple corresponding to environmental reflections remains. The mean of the ripple's amplitude in each case is calibrated and brought to the normalized value of the radiation pattern corresponding to its angle. Then, the EES is calculated for each data set as the half of the distance between the resulting ripple's maximum and minimum value, in linear units. The EES calculated in this way is then, again, added to the signal level reported in the radiation pattern for its corresponding angle, and the difference in dB caused by this addition is recorded. Finally, the mean of all recorded values is calculated for the derivation of the Std. uncertainty which, considering a V-shaped distribution, results in $0.36\,\mathrm{dB}$. For in situ measurements, the calculation of the effect of environmental reflections is, in many cases, not necessary. If a real application requires in situ testing at a certain distance, the environmental reflections, also present in the application, shall be considered as part of the measurement data and not of the uncertainty budget.

2) Finite Range Length: To assess the impact of the measurement distance not being infinite, i.e., the distance of real theoretical far field, a Spherical Wave Expansion (SWE) approach is used [15], [16]. Vectors of random Spherical Mode Coefficients (SMCs) are generated. From them, the far-field radiation pattern is calculated at $r = 350\,\mathrm{m}$, $r = 700\,\mathrm{m}$ and $r = \infty$. The radiation patterns are normalized and, using the one corresponding to $r = \infty$ as reference, the error is derived as the mean of the EES calculated in the same fashion of Eq. (1) using only amplitude data. This experiment is performed $N = 100$ times, each time redrawing the vector of SMCs. The error proves negligible, corresponding to a mean EES $< -60\,\mathrm{dB}$ in the main beam region (Std. uncertainty $< 0.01\,\mathrm{dB}$).

3) UAS Positioning: The positioning of the UAS is determined using GPS and it is known with an accuracy of circa $2\,\mathrm{cm}$, as described in Subsection II-B. In the case of measuring cuts, as opposed to rasters, the uncertainty is defined by a box with dimensions $30\,\mathrm{cm} \times 30\,\mathrm{cm} \times 30\,\mathrm{cm}$ surrounding the UAS due to wind influencing the drone out of its programmed flight plane. The resulting positioning accuracy is $\pm 0.025°$ for $r = 350\,\mathrm{m}$, and $\pm 0.0125°$ for $r = 700\,\mathrm{m}$. For the measured radiation pattern, this results in an equivalent Std. uncertainty $< 0.01\,\mathrm{dB}$.

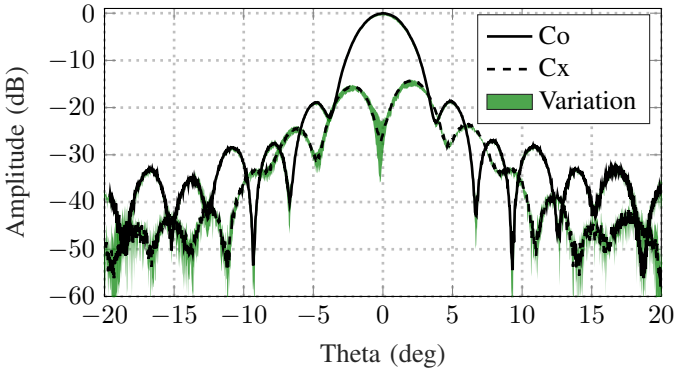

Fig. 7: Mean cut resulting of averaging 6 azimuth cuts acquired on the same day, together with the variations across all measured cuts.

4) Drift: RF components are sensitive to temperature and humidity. This aspect becomes more critical in outdoor measurements. To assess the effect of drift, static, single-point measurements have been performed at the beginning and the end of several measurement days. The observed signal variation has been processed to derive an average signal variation per time unit for each measurement day, which results in $\mathrm{Drift} = 0.35\,\mathrm{dB/hour}$ or around $\mathrm{Drift} = 0.006\,\mathrm{dB/minute}$. With this figure, the intra-measurement variation has been calculated using the average measurement duration per cut, which amounts to 3.5 minutes, resulting in a Std. uncertainty of $0.02\,\mathrm{dB}$.

V. Other Considerations

Outdoor measurements using UAS-APE raise concerns with regard to repeatability and the impact of random errors introduced by the own vibration of the UAS, as well as wind. These aspects are briefly discussed in this section.

A. Repeatability

To assess the repeatability of the measurements, measurements acquired on the same day are compared. In Fig. 7, the mean of 6 measurements of one of the AUT's main cuts at $r = 350\,\mathrm{m}$ is shown, together with the variation range across all 6 repetitions. It is assumed that the variations follow a zero-mean Gaussian distribution. While the variation is limited and the repeatability, thus, is high; averaging is used to further mitigate this effect.

B. Alignment: Vibrations, External Effects and Pointing Error

To evaluate the impact of random vibrations and external effects, such as wind, a single-point measurement at the AUT's boresight has been acquired. In this measurement, the UAS-APE acquires the same point for a determined time. In this experiment, the acquisition time was 5 minutes. A histogram showing the frequency distribution of the measured values during this time is shown in Fig. 8, normalized

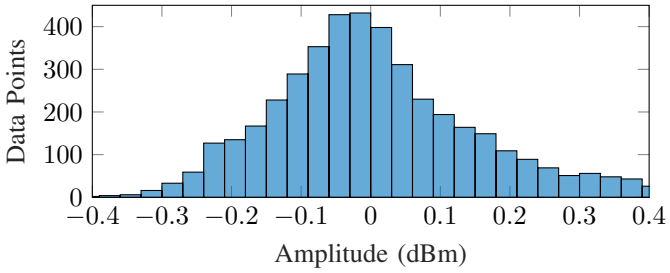

Fig. 8: Power distribution of points acquired at boresight during 5 minutes, normalized to their mean value.

to the mean. The uncertainty resulting from these effects, around $0.16\,\mathrm{dB}$ Std. uncertainty assuming a V-shaped distribution, is not included in the terms of the uncertainty budget discussed in Subsection IV-C, since it is considered to follow a zero-mean normal distribution and is compensated for with multiple measurements. However, a pointing error resulting from the capability of the payload to keep the alignment exists. The error performed by the current version of the payload is not quantified. To compensate systematic errors related to the direction of flight and other random pointing errors, the measurement cuts are acquired in both flight directions, e.g., from left to right and from right to left, or with an ascending and a descending motion. Thereafter, the computed mean of the measurements acquired in this way is used. To get an estimate of the difference between cuts acquired with different directions, the mean value of 3 azimuth cuts acquired from left to right is compared to the main value of 3 azimuth cuts acquired from right to left, both at $r = 350\,\mathrm{m}$. The difference of both can be modelled as a EES $< -45\,\mathrm{dB}$.

C. Elevation of the AUT

The elevation of the AUT with respect to ground has a direct influence on the resulting environmental reflections. Ideally for a directive antenna, the higher the elevation, the more reduced the environmental reflections, so the choice of elevation becomes a compromise with the possible (and legal) flight height. To estimate the effect of different elevation angles, multiple measurements of the main cuts for an elevation angle of El $= 35°$ and El $= 45°$ are compared. The difference between the mean cuts acquired for both elevation angles amounts to an EES $< -50\,\mathrm{dB}$.

VI. Conclusion

This work compares measurements acquired with a novel UAS-APE system with measurements performed at ESA-ESTEC's facilities, which were used as reference. The objective is to assess the accuracy of the UAS-APE system and to estimate the effect of error sources of concern in outdoor antenna measurements. The EES of the measured main cuts of the AUT is estimated to be EES $< -55\,\mathrm{dB}$ for the copolar component of the azimuth cut and the crosspolar component of the elevation cut, while it is EES $< -45\,\mathrm{dB}$ for the crosspolar component of the azimuth cut and the copolar component of the elevation cut.

A reduced uncertainty budget is made, estimating the impact of concerning error sources for outdoor ranges. Unsurprisingly, the largest uncertainty term is caused by environmental reflections, amounting to $0.36\,\mathrm{dB}$ of a total estimated combined uncertainty of $0.38\,\mathrm{dB}$ (1σ). While this term is indeed larger than its typical counterpart in anechoic chambers (around $0.01\,\mathrm{dB}$), it can be considered that, for the case of in situ measurements and real-application testing, the impact of this effect belongs to the measurement data, and not to the uncertainty. These results pave the way to a full, standardized uncertainty budget for UAS-APE systems and to an increased use thereof for outdoor measurements, with a special focus to in situ measurements.

References

[1] P. Dewdney, "SKA phase 1 system (level1) requirements specification," *SKA-OFF.SE.ARC-SKO-SRS-001-A, rev. 1*, November 2013.

[2] M. E. Asghar, F. Wollenschläger, C. Bornkessel, A. Griesche, and M. A. Hein, "Comparative analysis of spherical near-field automotive antenna measurement facilities," in *2019 13th European Conference on Antennas and Propagation (EuCAP)*, 2019, pp. 1–5.

[3] V. Platzgummer, V. Raida, G. Krainz, P. Svoboda, M. Lerch, and M. Rupp, "UAV-based coverage measurement method for 5G," in *2019 IEEE 90th Vehicular Technology Conference (VTC2019-Fall)*, 2019, pp. 1–6.

[4] J. DeRosa, "Full scale aircraft antenna measurements at the air force research laboratory, newport measurement facility," in *IEEE Antennas and Propagation Society International Symposium. 2001 Digest. Held in conjunction with: USNC/URSI National Radio Science Meeting (Cat. No.01CH37229)*, vol. 4, 2001, pp. 582–585 vol.4.

[5] A. D. Yaghjian, "An overview of near-field antenna measurements," *IEEE Transactions on Antennas and Propagation*, vol. 34, no. 1, pp. 30–45, 1986.

[6] O. Breinbjerg, "Spherical near-field antenna measurements — the most accurate antenna measurement technique," in *2016 IEEE International Symposium on Antennas and Propagation (APSURSI)*, 2016, pp. 1019–1020.

[7] *Evaluation of measurement data – Guide to the expression of uncertainty in measurement*. JCGM 100:2008, 2008.

[8] D. Gray, "How to choose an antenna range configuration," in *Antenna Measurement Techniques Association Symposium (AMTA)*, 2002, pp. 1–6.

[9] T. Fritzel, R. Strauß, H.-J. Steiner, C. Eisner, and T. Eibert, "Introduction into an uav-based near-field system for in-situ and large-scale antenna measurements (invited paper)," in *2016 IEEE Conference on Antenna Measurements Applications (CAMA)*, 2016, pp. 1–3.

[10] L. Washburn, E. Romero, C. Johnson, C. Gotschalk, and B. Emery, "Antenna calibration for oceanographic radars using aerial drones," in *2016 IEEE Conference on Antenna Measurements Applications (CAMA)*, 2016, pp. 1–4.

[11] M. García-Fernández, Y. Álvarez López, A. Arboleya, B. González-Valdés, Y. Rodríguez-Vaqueiro, M. E. De Cos Gómez, and F. Las-Heras Andrés, "Antenna diagnostics and characterization using unmanned aerial vehicles," *IEEE Access*, vol. 5, pp. 23 563–23 575, 2017.

[12] (2021, 7) Antenna laboratory, brochure. ESA / ESTEC. [Online]. Available: https://esamultimedia.esa.int/docs/technology/antenna-labbrochure_1.pdf

[13] J. Espeland and A. Buchi, "How drone technology will revolutionize satellite antenna testing," *Microwave Journal*, August 2020. [Online]. Available: https://www.microwavejournal.com/articles/34411-how-drone-technology-will-revolutionize-satellite-antenna-testing

[14] C. Parini, S. Gregson, J. McCormick, and D. Janse van Rensburg, *Theory and Practice of Modern Antenna Range Measurements*. IET Library, 2014.

[15] J. E. Hansen, *Spherical near-field antenna measurements*. IET, 1988, vol. 26.

[16] C. Culotta-López, R. Moch, R. Wilke, and D. Heberling, "On the influence of probe positioning errors due to mechanical uncertainties in spherical near-field measurements at terahertz frequencies in modern positioner systems," in *Photonics and Electromagnetics Research (PIERS)*. IEEE, 2019.